Size-control of iron oxide nanoparticles synthesized by thermal decomposition methods

Vladislava Fokina[†§], *Manuel Wilke*[†], *Martin Dulle*[†], *Sascha Ehlert*[†*], *Stephan Förster*[†§*]

[†]Jülich Centre for Neutron Science (JCNS-1/IBI-8), Forschungszentrum Jülich, 52425 Jülich, Germany
[§] Institute of Physical Chemistry, RWTH Aachen University, 52074 Aachen, Germany

[*]Address correspondence to: s.ehlert@fz-juelich.de, s.foerster@fz-juelich.de

ABSTRACT: The controlled synthesis of superparamagnetic iron oxide nanoparticles is crucial for a variety of biomedical applications. Among different synthesis routes thermal precursor decomposition methods are the most versatile, yielding monodisperse nanoparticles on the multi-gram scale. Recent *in situ* kinetic studies of the nucleation and growth processes during thermal decomposition routes revealed non-classical nucleation and growth paths involving amorphous precursor phases and aggregative growth steps. With the knowledge of this kinetic mechanism we systematically examined a range of different iron oxide heat-up synthesis routes to understand and conclude which methods allow good and reproducible size control over a range of relevant nanoparticle diameters. Using transmission electron microscopy (TEM) and small-angle X-ray scattering (SAXS) for the characterization of the nanoparticle size distribution we find that a set of solvents (1-octadecene, trioctylamine, docosane) provides access to a temperature range between 300 – 370°C allowing to synthesize monodisperse nanoparticles in a size range of 5 – 24 nm on large scale. We confirm that a thermal pretreatment of the iron oxide precursor is essential to achieve reproducible size control. We find that each solvent provides access to a certain temperature range, within which the variation of temperature, heating rate or precursor concentration allows to reproducibly control the nanoparticle size.

1. INTRODUCTION

Magnetic nanoparticles have received increasing attention in fundamental research as well as in a range of applications, particularly in medical diagnostics and therapy. Of great interest are superparamagnetic iron oxide nanoparticles (SPIONs) that are used as contrast agents in magnetic resonance imaging (MRI), in magnetic hyperthermia, for targeted drug delivery, and for bio separation[1].

SPIONs can be synthesized by different synthesis routes, among which thermal precursor decomposition methods are the most versatile, yielding monodisperse nanoparticles on the multi-gram

scale. Following the pioneering work of Park *et al*. [2], different variations of the thermal decomposition route have since then been developed. [2,3,4] They utilize ligand-assisted control over the nucleation and growth process to tailor nanoparticle size, shape and crystallinity. Thermal decomposition methods such as the heat-up method aim to separate the nucleation phase from the subsequent growth phase. If this is achieved, the variation of synthesis parameters such as temperatures, heating rate, precursor and ligand concentrations allows a size-controlled synthesis of monodisperse nanoparticles.

Recent investigations by time-resolved in situ X-ray scattering and electron microscopy of the nucleation and growth of nanoparticles [5,6] in the heat-up synthesis method showed that the nucleation and growth kinetics is rather complex, involving an amorphous precursor phase and aggregative growth, presumably by oriented attachment, until subsequent growth by monomer consumption yields the final nanoparticles. With the knowledge of this kinetic mechanism we here systematically examined a range of common variations of the iron oxide heat-up synthesis routes to understand and conclude which methods allow good and reproducible size control over a range of relevant nanoparticle diameters between 5 and 24 nm. Using transmission electron microscopy (TEM) and small-angle X-ray scattering (SAXS) for the characterization of the nanoparticle size distribution we find that a set of solvents (1-octadecene, trioctylamine, docosane), which provide access over a temperature range between 300 – 370°C, allows to synthesize monodisperse nanoparticles in a size range of 8 – 24 nm on large scale. We confirm that a thermal pretreatment of the iron oxide precursor is essential to achieve reproducible size control.

2. EXPERIMENTAL SECTION

2.1 Materials

Iron oxide precursor synthesis: Iron (III) chloride hexahydrate (Merck, ≥ 99.0%), sodium oleate (TCI, ≥ 97.0%), potassium oleate (TCI, >98.0%), n-heptane (Merck, ≥ 91.0%), ethanol (Merck, 96%), deionized water.

Particle surfactants: oleic acid (Aldrich, 90%; b.p. 360°C), oleylamine (Aldrich, 70%; b.p. 364°C), trioctilphosphine (Aldrich, 90%; b.p. 294°C)

Organic solvents for nanoparticle synthesis: 1-octadecene (Merck, ≥ 91.0%; b.p. 315°C), n-docosane (TCI, 99%; b.p. 369°C), trioctylamine (Aldrich, ≥92.5%; b.p. 365°C)

Purification step: tetrahydrofuran (Merck, ≥ 99.0%), ethanol (Merck, 96%) and acetone (Merck, ≥ 99.5%)

All components were used as received.

2.2 Transmission electron microscopy (TEM)

TEM measurements were performed using JEOL-F200 Multipurpose Electron Microscope. The standard procedure for sample preparation includes partial drying of diluted nanocrystal solution on a carbon-coated copper grid with following removal of excess solution..

2.3 Small angle X-ray scattering (SAXS)

SAXS experiments were held with the system "Ganesha-Air". The X-ray source is D2-Metalljet (Excillium) with a liquid metal anode operating at 70 kV and 3.57 mA with Ga-K_α radiation (λ = 0.1314 nm) providing a thick beam (< 100 µm) of high brilliance. X-ray optics (Xenocs) provides small and intense beam at the sample position, the beam size is adjusted with two pairs of slits depending on the detector distance. Samples were measures in borosilicate capillaries (d = 2 mm) at room temperature (T = 24 °C). If not stated otherwise data was radial averaged, normalized with respect to measurement time and transmission and the solvent as background subtracted.

2.4 SAXS and TEM data analysis

Small angle scattering curves were fitted with "polydisperse core-shell sphere" model using Jscatter software [3]. The model allows to increase quality of fits not only because of included polydispersity parameter, also because of the shell parameter as iron oxide particles are stabilized with surfactant, which contributes overall scattering.

For the determination of mean particle diameters in the TEM images we used the software ImageJ. This software can also be used to prepare histograms of nanoparticle size distributions. Exemplarily, we prepared histograms (see Fig. S3 in Supporting Information) for the TEM-images displayed in Fig. 3 for a comparison between the mean radii determined by SAXS and TEM. We observe that the nanoparticle core radii determined by SAXS are systematically larger by ca. 0.2 – 0.3 nm compared to the mean nanoparticle radii determined by TEM. We attribute this to the fact that the mean radii determined by SAXS represent a weight average, which is slightly larger compared to the number average determined by TEM. Furthermore, a reduced crystallinity of the nanoparticles in their outermost atomic layers can reduce their TEM-contrast at their periphery, also leading to slightly smaller apparent radius. Throughout the manuscript, for comparison of the synthetic methods, we therefore consider the mean radii determined by SAXS because they refer to an average over a very large number of particles with good statistics.

2.5 The thermal decomposition route

The synthesis of SPIONs was carried out by thermal decomposition of iron oleate as in the previously reported procedure by Park *et al*. [4]. The general procedure uses a mixture of precursor, organic solvent

and ligand. The synthesis of the precursor is described in detail in Section 3.2. In the standard procedure iron oleate is used as the precursor, oleic acid as the ligand, and 1-octadence as the solvent. A typical reaction mixture consists of 125 ml of 1-octadecene, 3.2 ml oleic acid (10 mmol), and 18 g of Fe(III)-oleate (20 mmol, 2:1 molar ratio to oleic acid). Thermal decomposition is performed under Argon atmosphere at a starting temperature of 100°C, a heating rate of 3.3 °C/min, an end temperature of 320°C, and rapid cooling down to room temperature after an annealing time of 30 minutes. Heating rates are varied between 1 – 10 °C/min.

3. RESULTS AND DISCUSSION

3.1 Time-resolved small-angle X-ray scattering experiments

Small-angle X-ray scattering (SAXS) was used to characterize the size and size distribution of the obtained nanoparticles in solution, and in one case during the synthesis. Fig. 1 a-d show typical measured SAXS-curves for iron oxide nanoparticles. The scattering curves show a well-defined Guinier plateau at small values of the scattering vector q, followed by the q^{-4} Porod regime featuring several formfactor oscillations. These allow to determine the mean particle diameter and polydispersity with good accuracy.

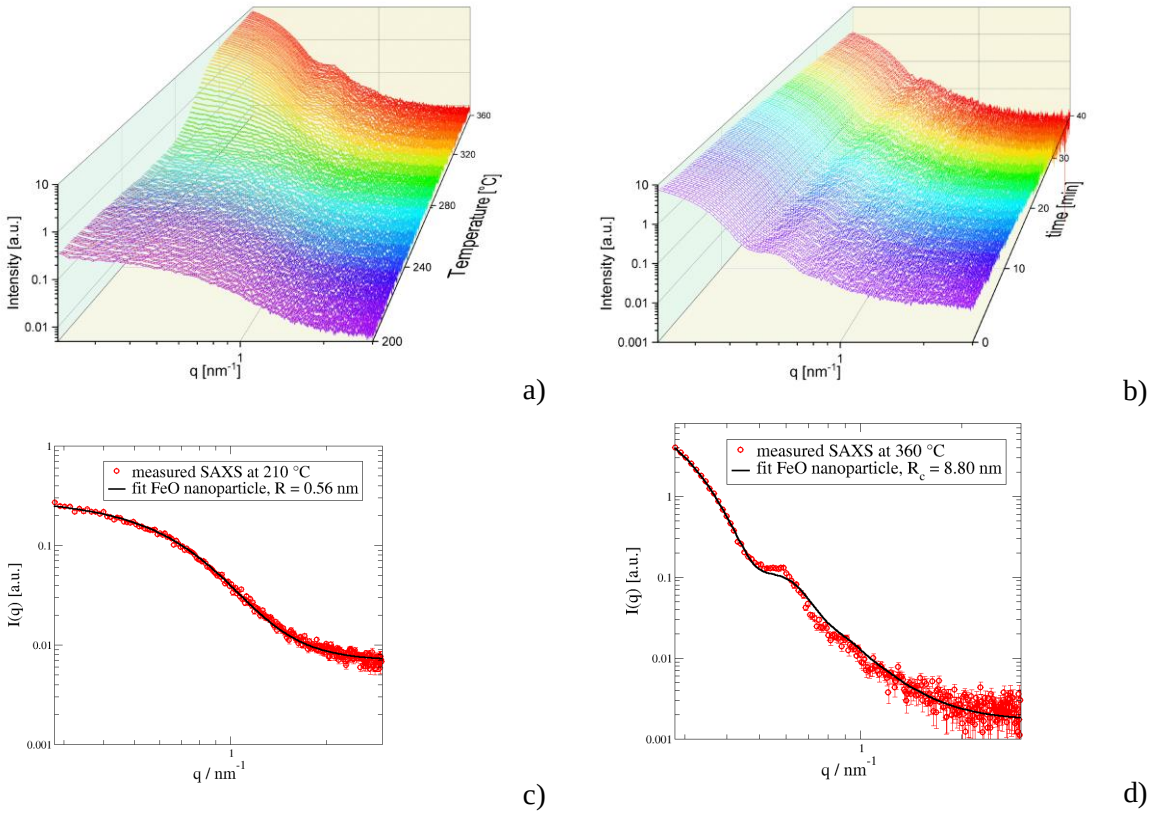

Figure 1. Typical SAXS-curves measured during the heating phase (a) and subsequent annealing phase (b) of the heat-up synthesis of iron oxide nanoparticles. (a) Waterfall plot of the SAXS curves measured during heating of the reaction mixture in trioctylamine from 200 °C to 360 °C, i.e. during particle growth, at the standard heating rate of 3.3°C/s, b) waterfall plot of SAXS curves measured for a subsequent annealing phase at 360 °C to show that no further growth is observed. c) and d) show selected SAXS curves at 210 °C and 360°C with fits to Eqs. (2, 3) (solid lines).

For a quantitative analysis we use an analytical description of the scattering curve. The scattering intensity $I(q)$ is given by

$$I(q) = I_0[\mathrm{P}](\Delta b)^2 V^2 P(q) \tag{1}$$

where I_0 is the primary X-ray beam intensity, [P] the particle concentration, Δb the scattering contrast between particle and solvent, and V the volume of the particle. $P(q)$ is the formfactor of the particle, for which we assume a core/shell structure, where the iron oxide nanoparticle forms the core and the ligand forms the shell. In the limit $q \to 0$ the formfactor approaches $P(q) \to 1$. This allows to calculate a relative particle concentration $N_{rel} = I(0)/V^2$ from Eq. (1), which during the nucleation process first increases and later decreases due to aggregative growth (See Fig. S1 in the Supporting Information).

The formfactor for polydisperse homogeneous spherical particles is given by

$$P(q) = \frac{9}{(qR)^6}(\sin(qR) - qR\cos(qR))^2 \tag{2}$$

where R is the particle radius. To take into account polydispersity, the formfactor $P(q)$ is averaged over a size as outlined in ref. [5]. This formfactor is used to describe the scattering curves in the initial phase of the heat-up synthesis as shown in Fig. 1c.

In the subsequent phase the scattering curves are described by the formfactor of spherical core/shell particles with homogeneous core and shell. The formfactor is given by

$$P(q) = \frac{3}{V_s}\left[V_c(\rho_c - \rho_s)\frac{\sin(qR_c) - qR_c\cos(qR_c)}{(qR_c)^3} + V_s(\rho_s - \rho_{solv})\frac{\sin(qR_s) - qR_s\cos(qR_s)}{(qR_s)^3}\right] \tag{3}$$

where V_s is the volume of the whole particle, V_c is the volume of the core, R_s is the radius of the particle, R_c is the radius of the core, ρ_c , ρ_s and ρ_{solv} are the scattering length density of the core, shell and solvent. The ligand shell contributes significantly to the scattering intensity at high q. The shell thickness between 1.7 and 3 nm is in good agreement with the expected thickness of ligand monolayers.

During the development of a new *in situ* SAXS high-temperature reactor we were able to perform a first experiment using a high-boiling solvent trioctylamine. For the *in situ* experiment the reaction mixture was preheated to 200 °C. Below a temperature of 200°C we did not observe any changes of the reaction mixture or indications for particle formation. The measured SAXS curves for the heating process from

200 °C to 360 °C (Fig. 1 a) show a typical Guinier region and a high-*q* decay typical for very small particles. Fig. 1 c shows the SAXS curve measured at 210 °C. We could fit this curve with a model of polydisperse spheres. The obtained radius is 0.56 nm, suggesting the presence of small stable iron-ligand species. All data until 280 °C give the same radius when fitted. Above 280°C growth of monodisperse particles can be observed. After the heating ramp from 200 – 360°C the reaction mixture was stirred for 40 min at 360 °C as shown in Fig. 1 b, where a slight decay of the scattering intensity with time is observed. Figure 1 d shows the SAXS curve measured at 360 °C. We clearly observe the shift of the first minimum of the scattering curve to lower *q*-values during the second phase above 280°C, indicating the growth of the narrow disperse iron oxide nanoparticles.

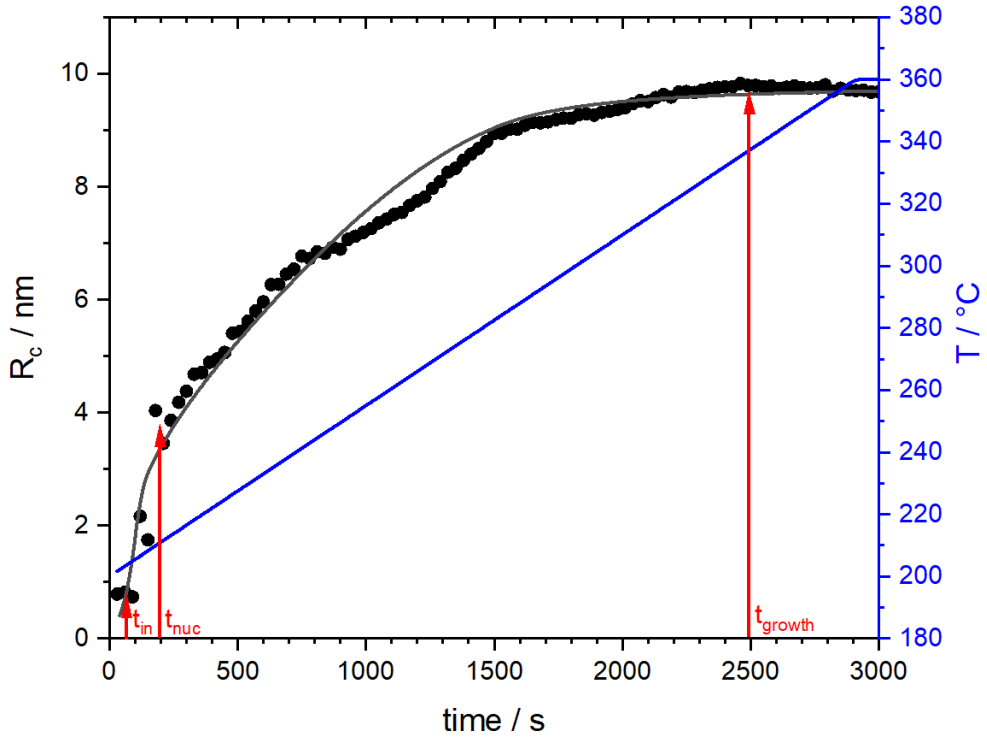

Figure 2. Measured core radii for the kinetic experiment shown in Fig. 1 together with a model calculation (solid line) using the kinetic scheme from Eq. (4), and the corresponding temperature. The calculated curve well describes the main features of the growth curve including the induction time until the time t_{in}, the time period for the burst nucleation until the time t_{nuc}, the subsequent growth phase until the time t_{growth}, and the final plateau value of the particle radius.

Fig. 2 shows the measured core radii as a function of time as determined from the scattering curves in Fig. 1 a and b. We observe the onset of nucleation to occur after 100 s, followed by a sharp initial

increase of the radii to 4 nm during the next 100 seconds. Subsequently the particles grow at lower growth rates to finally reach a radius of 9.8 nm after 2000 seconds.

The main features of the growth curve including the induction time of 100 seconds, the nucleation phase in the subsequent 100 seconds and the following growth and saturation phase can be well described by a nucleation and growth model as shown by the solid line in Fig. 2. The corresponding kinetic considers (i) the $Fe(OA)_3$ iron oleate precursor decomposition with a rate constant k_1, (ii) a classical nucleation step with the rate constant k_{nuc}, (iii) particle growth by consumption of precursor with a growth rate k_{gr}, and (iv) aggregative growth steps, e.g. by oriented attachment, with a rate constant k_{agg}

$$Fe(OA)_3 \xrightarrow{k_1} Fe(OA)_m \tag{4}$$

$$Fe(OA)_m \xrightarrow{k_{nuc}} (FeO_x)_{nuc}$$

$$P_J \xleftrightarrow{k_{gr,J}} P_{J+1}$$

$$P_J + P_{J'} \xrightarrow{k_{agg}} P_{J+J'}$$

The model is described in detail in ref. [6] and the main parameters are summarized in the Supporting Information. For the present study we note that the model captures the main features of the iron oleate heat-up synthesis kinetics as shown in Fig. 1 a, b, using the exact same thermodynamic and kinetic parameters used in the previous kinetic study [6], which themselves well compare to studies reported earlier in literature. In the previous study we used 1-octadecence as a solvent, whereas in Fig. 1,2 trioctylamine was the solvent. The only difference in parameters compared to the study in 1-octadecene is that for trioctylamine we used a smaller precursor decomposition rate constant of $k_{1,0}$ =6.0·10^2 mol/m^3·s compared to $k_{1,0}$ =3.0·10^5 mol/m^3·s for 1-octadecene, and a growth rate constant of $k_{gr,0}$ = 3.3·10^5 m/s which is slightly larger than for 1-octadence where the values were in a range of $k_{gr,0}$ = 5.8 - 17·10^4 m/s depending on temperature. In the Supporting Information we also consider the temporal evolution of the relative particle numbers N_{rel} which decreases during the reaction due to aggregative growth steps. The measured shell thickness R_s varies between 1.7 nm and 3 nm when R_c reaches a size bigger than 4.5 nm. This is in good agreement with the thickness of a ligand shell.

The knowledge that the nucleation and growth kinetics at higher temperatures up to 360°C in the high-boiling solvent trioctylamine is the same as for 1-octadence at lower temperatures of 280 – 320°C allows us to better rationalize the influence of different experimental parameters to conclude on the most favorable experimental conditions to synthesis monodisperse iron oxide nanoparticles over a wide range of diameters. The reason for the smaller decomposition rate of trioctylamine could be a better stabilization of the iron precursor by the amine group.

3.2 Iron oleate precursor synthesis

We found that one essential parameter for a reproducible synthesis of superparamagnetic iron oxide nanoparticles (SPIONs) is the final treatment of the synthesized iron oleate complex. It can be synthesized via the reaction of iron chloride and sodium oleate 1, 2 or using iron oxides dissolved in oleic acid [8,9]. In the present work the synthesis of the iron-oleate precursor was performed using reaction of iron (III) chloride and sodium oleate.

Since the synthetic procedure is important, we here describe the synthesis steps with the relevant details. In a typical procedure 32.4 g of iron chloride ($FeCl_3 \cdot 6H_2O$) and 109.5 g of sodium oleate were mixed and dissolved in a mixture of 120mL of distilled water, 160 mL of ethanol and 280 mL of heptane. The solution was stirred at 70 °C for 4 hours. Afterwards the brownish organic phase was washed 3 times with distilled water in a separatory funnel. Subsequently, heptane was removed in a rotary evaporator, followed by drying the resultant iron oleate at 60 °C for 3 days, until the substance became highly viscous. The iron oleate complex was further stored in a vacuum oven.

Systematic studies of the dependence of SPION size-control on the iron oleate drying time were reported earlier[10]. An increase of the particle size with increasing precursor drying time was observed. Using FTIR-spectroscopy and DSC-analysis, the authors detected a decreasing amount of weakly ligand-bound Fe centers with increasing drying time. Therefore, we investigated the influence of iron oleate drying time on the size, size distribution, and shape of the obtained SPIONs for our iron oleate precursors as well.

One type of synthesis was performed with a “fresh” precursor which was only dried in a rotary evaporator. The second type of reaction was done with iron oleate dried for 3 days at 60 °C. Afterwards both precursors were stored in a vacuum oven at room temperature. We observed that nanoparticles synthesized with the “fresh” iron oleate in 1-octadecene (ODE) as a solvent had a radius of 3.6 nm (Fig. 3 a). The same synthesis was repeated after one and two weeks, where nanoparticles with radii of 4.3 and 5.5 nm were obtained, respectively (Fig. 3 b, c). The analysis of the SAXS curves with a polydisperse core/shell-sphere model (Fig. 3 d) similarly showed that the average nanoparticle diameters increased with the second and the third synthesis, and that the polydispersity decreased in the same order. Although the quality of the nanoparticles is excellent, there is the disadvantage of the low reproducibility of synthesis because the particle diameter can only be varied rather uncontrollably.

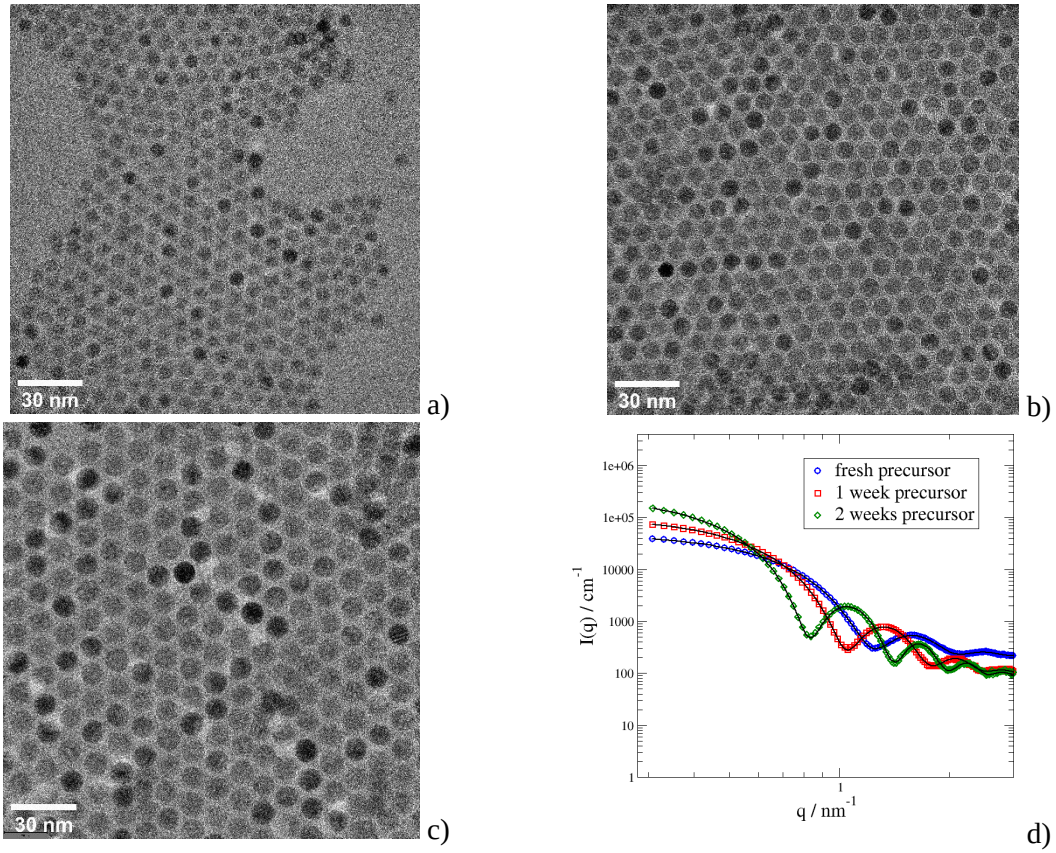

Figure 3. TEM images of iron oxide nanoparticles synthesized from an iron oleate precursor which was a) dried only in a rotary evaporator, b) dried additionally for 1 week in the vacuum oven, and c) dried additionally for 2 weeks in the vacuum oven. d) shows the measured SAXS curves of the synthesized nanoparticles together with core/shell model fits indicated by the solid lines. The core radii determined by the fits are R_c = 5.5 nm (green curve), 4.3 nm (red curve) and 3.6 nm (blue curve) respectively.

To achieve a more reproducible synthesis and larger particle diameters, we used the second type of synthesis route, i.e. with the iron oleate precursor dried in a water bath at 60 °C. As shown in Fig. 4a, the nanoparticles reached a radius of 6.6 nm. A synthesis repeated after two months from the same iron oleate gave particles with a radius of 7.0 nm. (Fig. 4b), which indicates good reproducibility of the synthesis, if well-dried iron oleate precursor is used. In light of the investigations reported in ref. [10] we conclude that weakly bound iron centers form weakly stabilized nuclei that are nucleated at higher supersaturation and thus in a larger number, resulting in smaller nanoparticles after growth. In all following investigations we therefore used iron oleate prepared with the additional drying process at 60°C for a well reproducible synthesis.

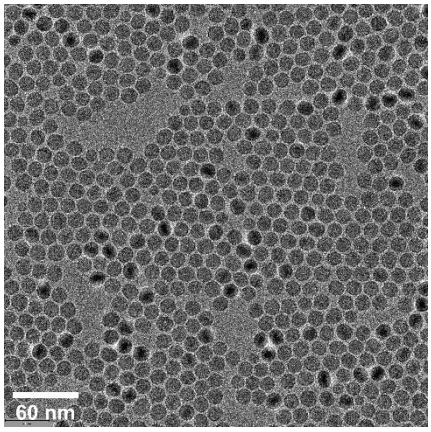

a)

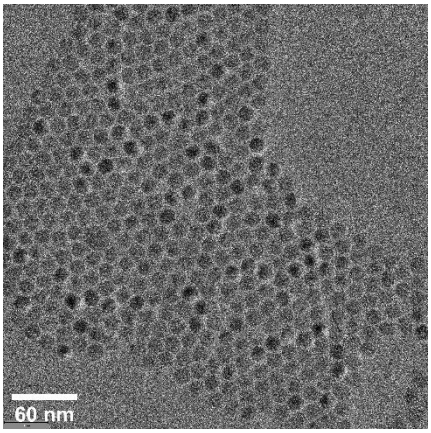

b)

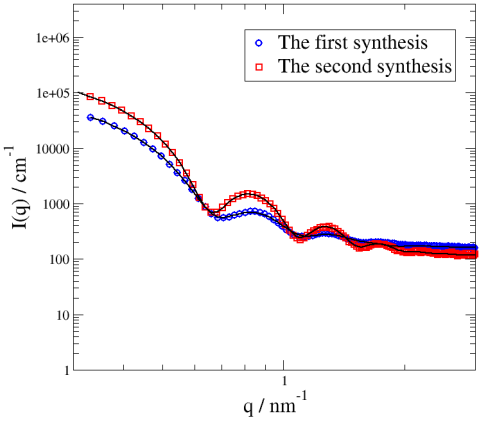

c)

Figure 4. TEM images of iron oxide nanoparticles synthesized from an iron oleate precursor that was carefully dried in a water bath at 60 °C: a) the first synthesis, b) the second synthesis, repeated after one month. c) shows the measured SAXS curves of the synthesized nanoparticles together with core/shell model fits indicated by the solid lines. The determined core radii are R_c = 6.6 nm (blue curve) and 7.0 nm (red curve), respectively, showing the good reproducibility of the synthesis.

3.3 Influence of the main synthesis parameters

A) Heating rate

Having an adequate iron oleate precursor synthesis established, we changed the heating rate as the first parameter for varying the nanoparticle radius, using 1-octadecene as the solvent and an end temperature of 320°C. We changed the heating rate of the reaction solution from the standard (3.3 °C /min) to a slower (1.6 °C /min) and a higher heating rate (10 °C /min), leaving all other standard parameters fixed (See Sec. 2.1). We observe that using the standard heating rate of 3.3°C/min leads to highly monodisperse particles with radii of 4.3 nm (Fig. 5 a). A lower heating rate increases the radius slightly to 4.4 nm with an increased polydispersity (Fig. 5 b). The higher heating rate broadens the size distribution (Fig. 5 c).

Generally, lower heating rates lead to larger particles. According to the nucleation and growth kinetic scheme [6] this is due to the lower number of nuclei formed, which upon consumption of the precursor grow to larger particles. The lower number of nuclei is related to the fact that nucleation for lower heating rates occurs already at lower temperatures, where the nucleation rates are smaller.

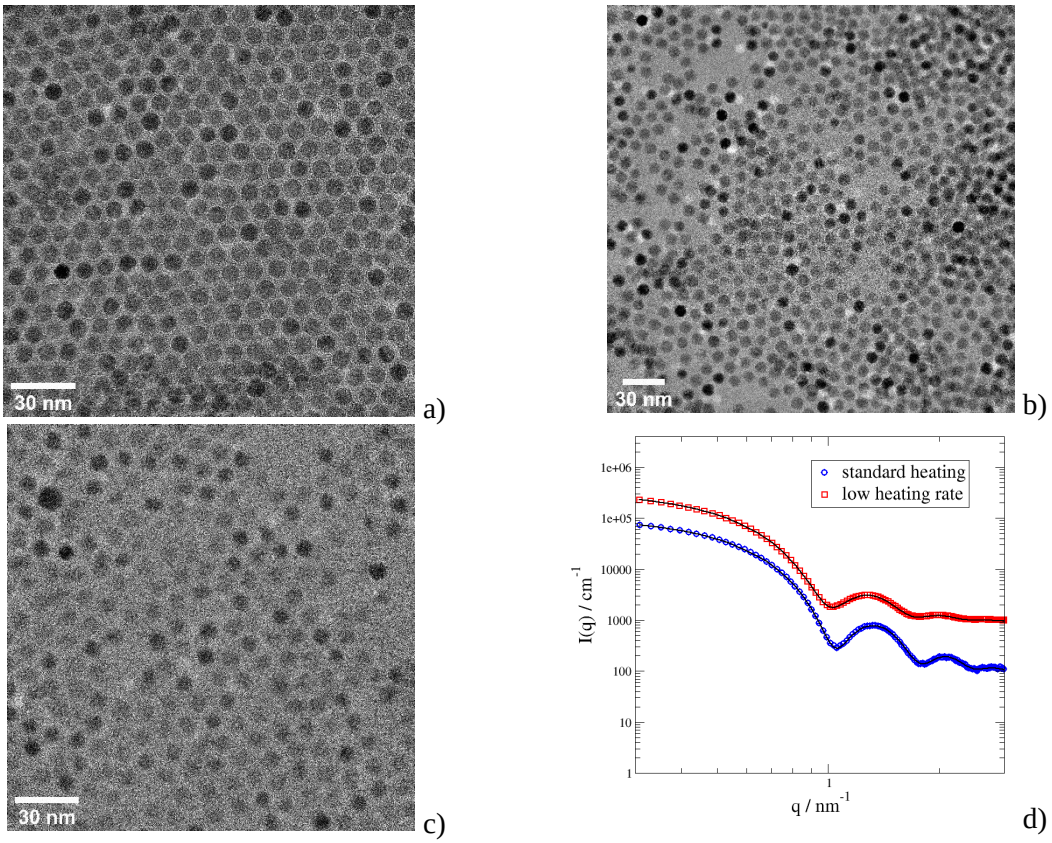

Figure 5. TEM images of iron oxide nanoparticles formed at different heating rates: a) standard heating rate 3.3 °C /min, b) lower heating rate 1.6 °C /min, c) and higher heating rate 10 °C /min. d) shows the measured SAXS curves of the synthesized nanoparticles together with core/shell model fits indicated by the solid lines. The determined core radii are R_c = 4.3 nm for standard heating rate (blue curve) and 4.4 nm for lower rate (red curve).

B) Annealing time

The annealing time at the final plateau temperature is a parameter that also plays a role in the nanoparticle synthesis. When performing the synthesis in 1-octadence with the standard heating rate of 3.3°C/min and 320°C as the plateau temperature, we observe that 30 min of annealing yields monodisperse nanoparticles with a radius of 4.3 nm (Fig. 6 a). After 60 min the size distribution broadens. The size distribution then becomes bimodal, with a small fraction of small nanoparticles with radii of 2 nm and large nanoparticles with radii of 6.5 nm. An annealing time of 0 minutes, i.e. immediate termination of the reaction right after reaching the final temperature of 320 °C, results in

nanoparticles with broader size distributions between 2 to 4 nm radius, because the growth process that focuses the size distribution after the aggregation steps [6] is not yet completed (Fig. 6 c). In all cases we obtain spherical nanoparticles. As will be outlined below, SPIONs synthesized with a plateau temperature of up to 360°C in a high boiling solvent (docosane) become spherical and monodisperse already after 3 min of annealing[11], because the growth rates are sufficiently high. Therefore, we conclude that the annealing time should be just long enough to complete growth.

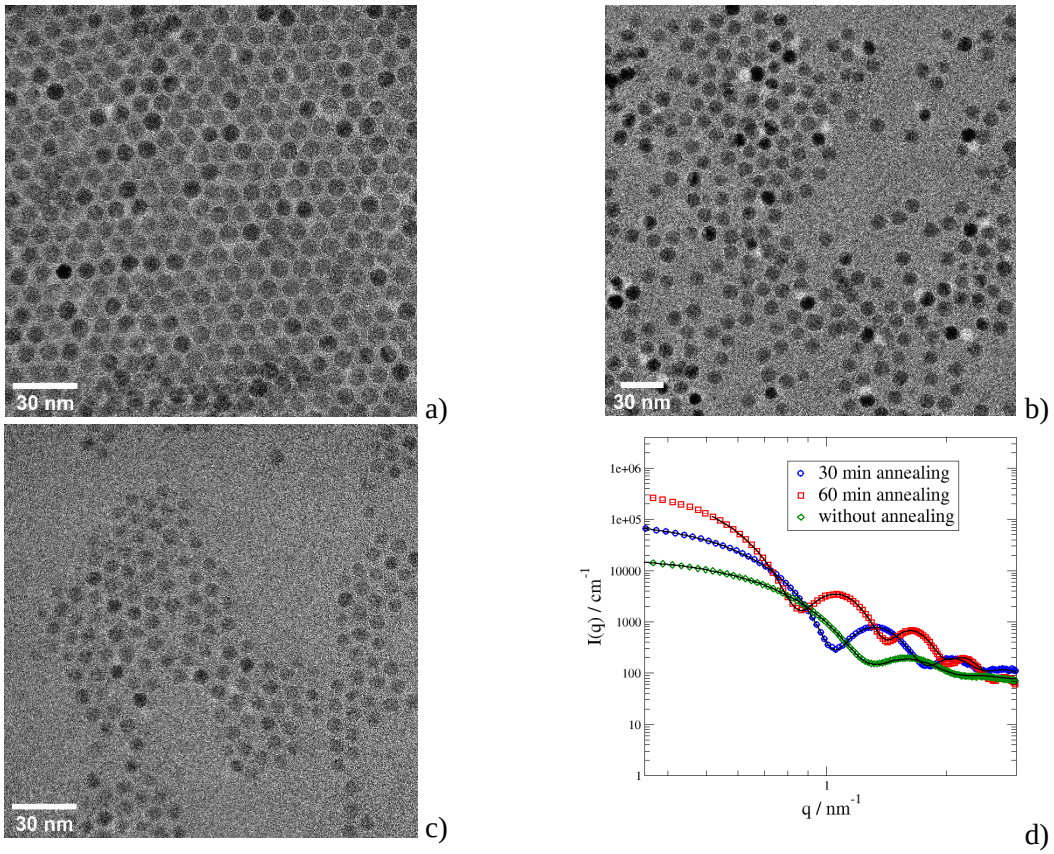

Figure 6. TEM images of iron oxide nanoparticles synthesized at 320 °C during different annealing times: a) 30 min, b) 60 min, c) 0 min. d) shows the measured SAXS curves of the synthesized nanoparticles together with core/shell model fits indicated by the solid lines. The determined core radii are R_c = 4.3 nm (blue curve), 5.3 (red curve) nm and 3.4 nm (green curve), respectively.

C) Ligand type

Oleic acid is the most common ligand for SPIONs surface stabilization [4,7,10,12] . Usually, the variation of the ligands is used to control the shape of SPIONs, mainly via the variation of ratio of sodium/potassium oleate and oleic acid ligands[12,13]. In our case we only focus on the synthesis of spherical nanoparticles.

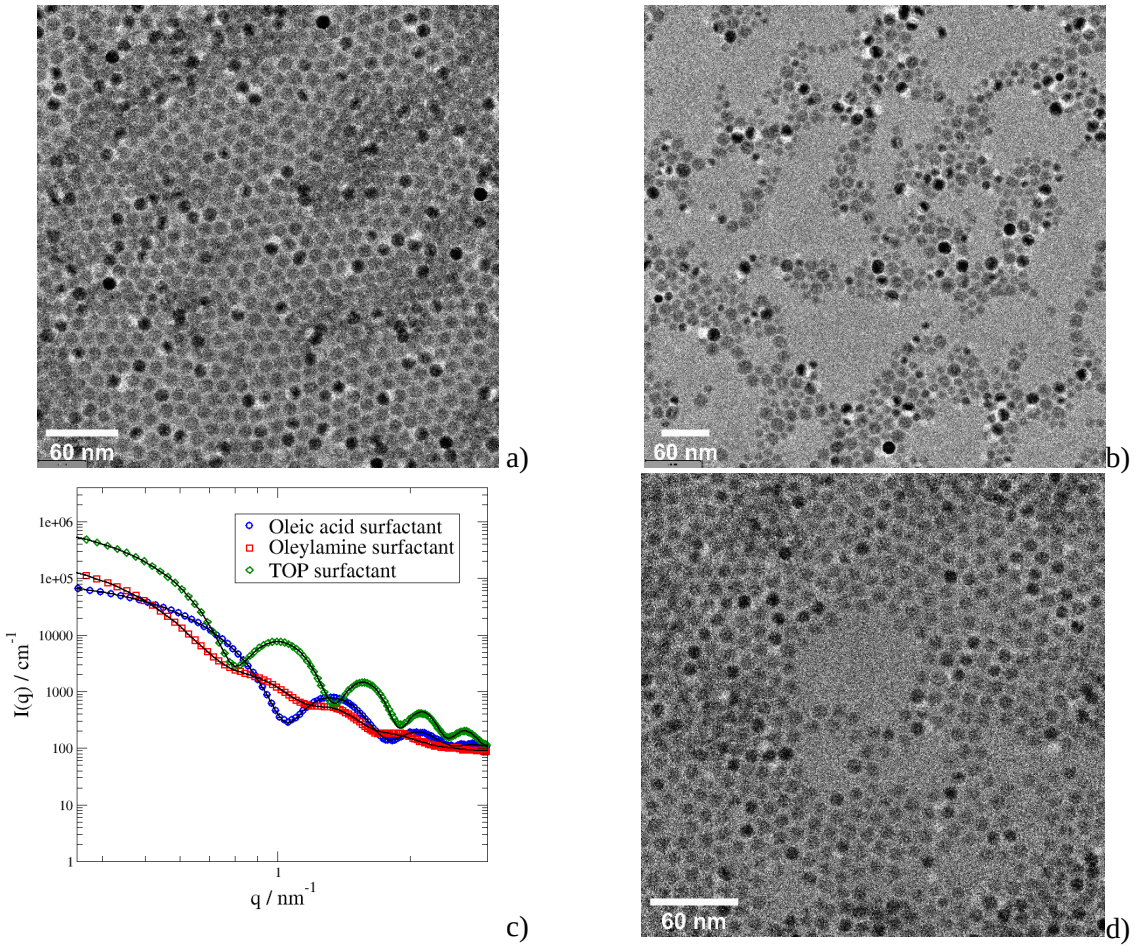

Figure 7. TEM images of iron oxide nanoparticles stabilized with a) trioctylphosphine and b) oleylamine, c) shows the measured SAXS curves of the synthesized nanoparticles together with core/shell model fits indicated by the solid lines. The determined core radii are R_c = 5.7 nm (green curve), 5.5 nm (red curve) and 4.4 nm (blue curve) respectively d) particles without extra surfactant.

We therefore investigated trioctylphosphine (TOP) as another possible ligand. The synthesis was carried out according to the standard procedure, i.e. with 1-octadecene as the solvent, with a 20 mmol concentration of the iron oleate, a heating rate of 3.3°C/min, and an end temperature of 320°C. As shown in Fig. 7 a we obtained monodisperse spherical nanoparticles with radii of 5.7 nm. This is larger compared to oleic acid as a ligand, where particle radii of 4.4 nm are obtained for the standard procedure. When using oleylamine as a ligand (Fig. 7 b), polydisperse nanoparticles with different shapes were obtained. A complete absence of extra surfactant (Fig. 7. d) leads to nanoparticles with increased polydispersity with an average radius of around 4.5 nm.

The role of the ligand is to stabilize the nuclei during their formation and to stabilize the growing nanoparticles. Different ligands have different binding strengths to the nanoparticle surface. [9, 14] Usually, there is an optimum binding strength where nuclei are sufficiently stabilized by the ligand, but not to a degree that the ligand shell subsequently acts as a barrier that retards particle growth. Oleic acid interacts with iron oxide via hydrogen bounds Fe-O···H ··· O=C-. TOP, which is a weak base in the HSAB-sense, interacts with the hard acid Fe^{3+} at the iron oxide surface via intermediately strong Fe···P-C- bonds. Oleylamine, is a hard base in base in the sense of the Hard Soft Acid Base (HSAB) concept which has stronger binding via Fe···N-R-bridges and therefore leads to smaller and more polydisperse nanoparticles. Therefore, oleic acid and TOP are excellent ligands. TOP can be used to obtain larger nanoparticles compared to oleic acid as the ligand, both with good and reproducible control of the particle radius and narrow size distributions.

D) Variation of precursor concentration

We also investigated large variations of the iron oleate precursor concentration. Keeping the Fe/ligand ratio constant at 2:1, we used a 3-times reduced amount of iron oleate (6g) and a 9-times increased amount of iron oleate (54 g) in the same volume of solvent (125 ml). With the 3-fold reduction of the iron oleate precursor concentration polydisperse nanoparticles with an average radius of 4.7 nm are obtained (Fig. 8a). The 9-fold increased iron oleate concentration leads to nanoparticles with an average radius of 7.0 nm (Fig8b). We observe that reducing the concentration decreases the growth rate to a degree such that growth is slow leading to smaller and more polydisperse nanoparticles. The slightly larger size and increased polydispersity observed at low precursor concentration appears to result from a slower nucleation rate. The larger size at higher precursor concentration likely is related to larger growth rates with faster monomer addition, thus leading to larger particles sizes.

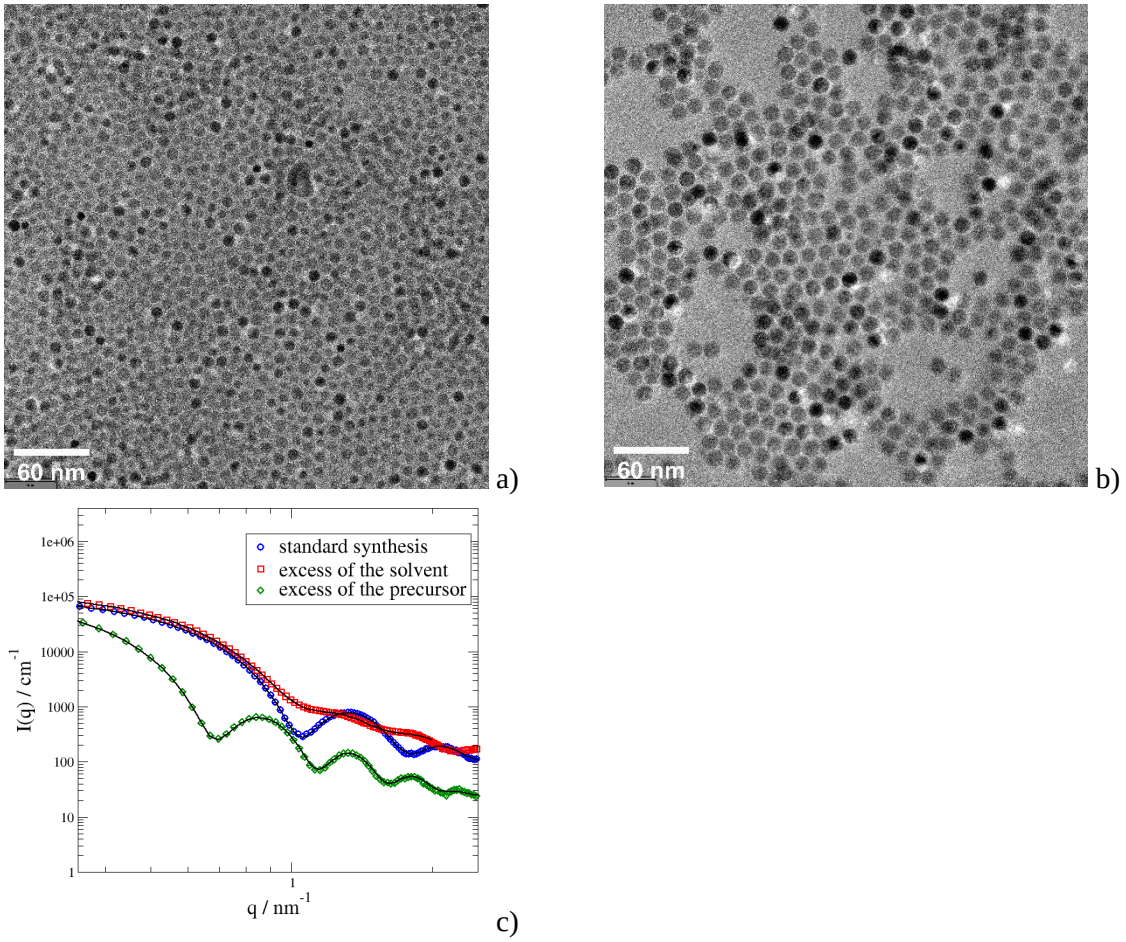

Figure 8. TEM images of iron oxide nanoparticles synthesized from a solution with a) excess of solvent, b) excess of precursor, c) shows the measured SAXS curves of the synthesized nanoparticles together with core/shell model fits indicated by the solid lines. The determined core radii are R_c = 4.7 nm (red curve), 6.7 nm (green curve) and 4.3 nm (blue curve), respectively.

3.4 The use of high-boiling point solvents.

The variation of the standard synthesis parameters provides an opportunity for a fine control of spherical nanoparticles sizes. The main way to significantly increase nanoparticle diameters is by the use of higher temperatures in high boiling point solvents for the nanoparticle synthesis[4,9,11]. Whereas the precursor concentration (20 mmol) and the heating rate (3.3°C/min) are according to the standard procedure, this change requires to adjust other parameters such as the end temperature, annealing time or the amount of compounds and demands some alterations of the synthesis set up depending on each solvent.

The standard solvent 1- octadecene (bp = 315 °C), which was used for the previous set of experiments, allows to synthesize nanoparticles with diameters of up to 14 nm diameter in case of well-dried iron oleate precursors at an end temperature 320 °C. These nanoparticles have a magnetite phase and a monocrystalline structure (Fig. 9).

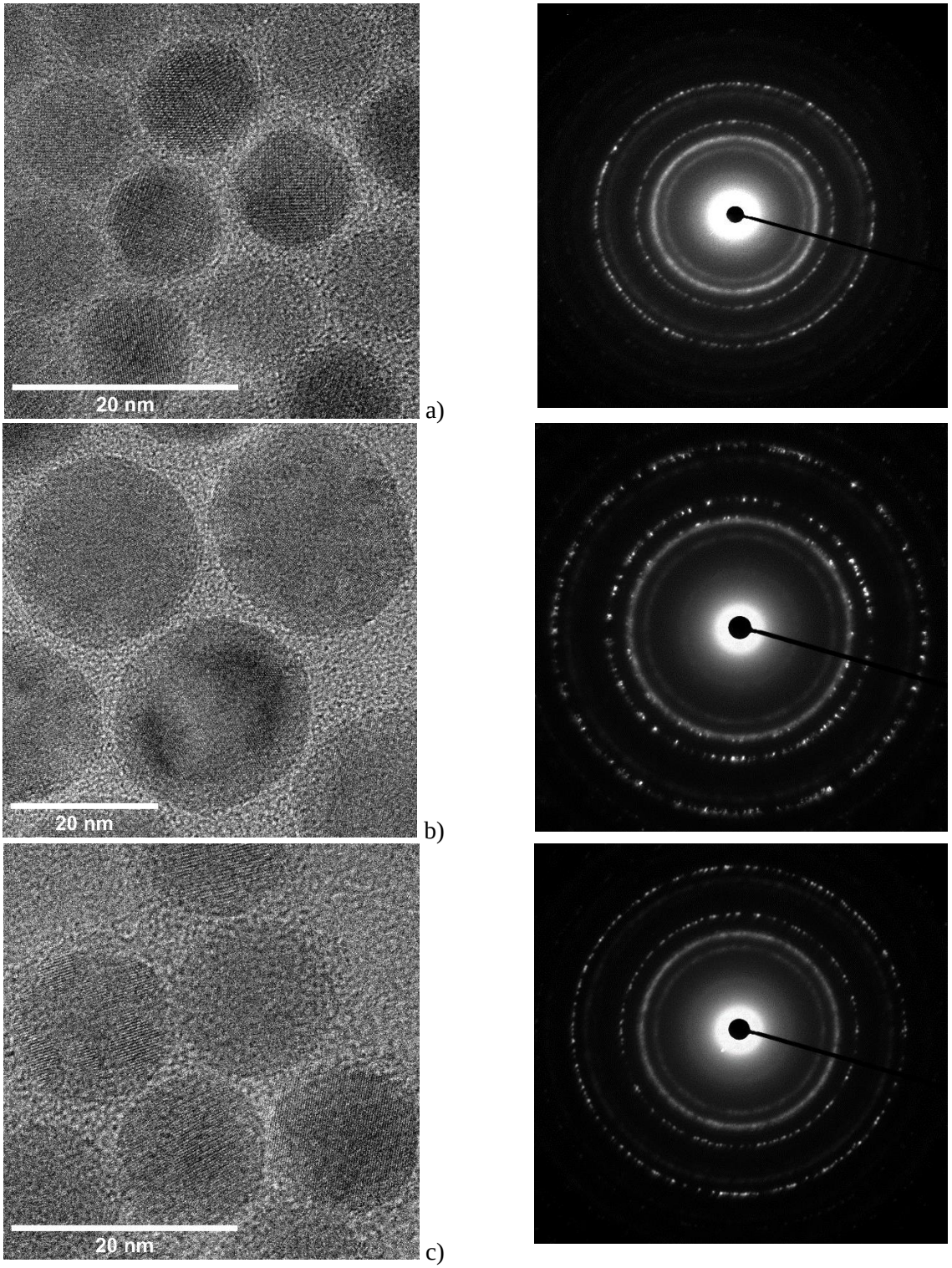

Figure 9. TEM image at high magnification and selected area electron diffraction patterns (SAED) of particles formed in a) 1-Octadecene, b) Docosane, and c) Trioctylamine.

Docosane

Using docosane as a higher boiling point solvent (bp = 368.6 °C) and following the procedure described by Bronstein and co-workers[11], it is possible to reach a nanoparticle radius of 10.5 nm (Fig. 10 a). The diameters can be varied by changing the amount of solvent in the precursor solution. Increasing the concentration 3-fold, by using 10mL instead of 30mL solvent, reduces the radius to 9.8 nm (Fig. 10 b). We note that the purification step is tricky for particles which were synthesized in docosane. In a usual purification procedure the resulting particles are precipitated by adding acetone to the mixture. Afterwards the solvents are removed by decantation and the particles are redispersed in THF. This procedure is repeated at least two times with ethanol until the supernatant is transparent. For particles, which were synthesised in docosane, two additional precipitation steps with ethanol at 60°C are necessary, because docosane (m.p. > 60°C) is solid at room temperature.

One of the main peculiarities of the synthesis with docosane is that the nucleation step is shifted to high temperatures. There is hardly any difference in the resultant particle size distribution if the starting reaction temperature is either 60 °C, 100 °C or even 300 °C. The starting amount of material for synthesis also does not influence the SPIONs size: upscaling of the amount of all compounds by factor of 4 for the procedure described by authors[11] allows to get the same size range with a radius of 12.1 nm. (Fig. 10 c). Therefore, the use of docosane as a solvent provides a highly reproducible synthesis of monodisperse nanoparticles, where the particle size can be controlled by the precursor concentration. We observe from the TEM-images that the particle shape slightly deviates from a spherical shape. Also, the nanoparticles synthesized in docosane have a magnetite phase and a monocrystalline structure (Fig. 9b).

The presence of several iron oxide phases was reported for particles synthesized at high temperatures. XRD measurements show a co-existence of Wüstite (FeO) and Spinel (most likely Fe_3O_4)[11]. It was argued that the Wüstite phase in iron oxide core-shell structures is more pronounced in larger particles because of longer diffusion path for the oxidation process[15]. The field dependent magnetisation measurements prove superparamagnetic behaviour of FeO-Fe_3O_4[10] particles and even better magnetic properties in comparison to one-component SPIONs [16].

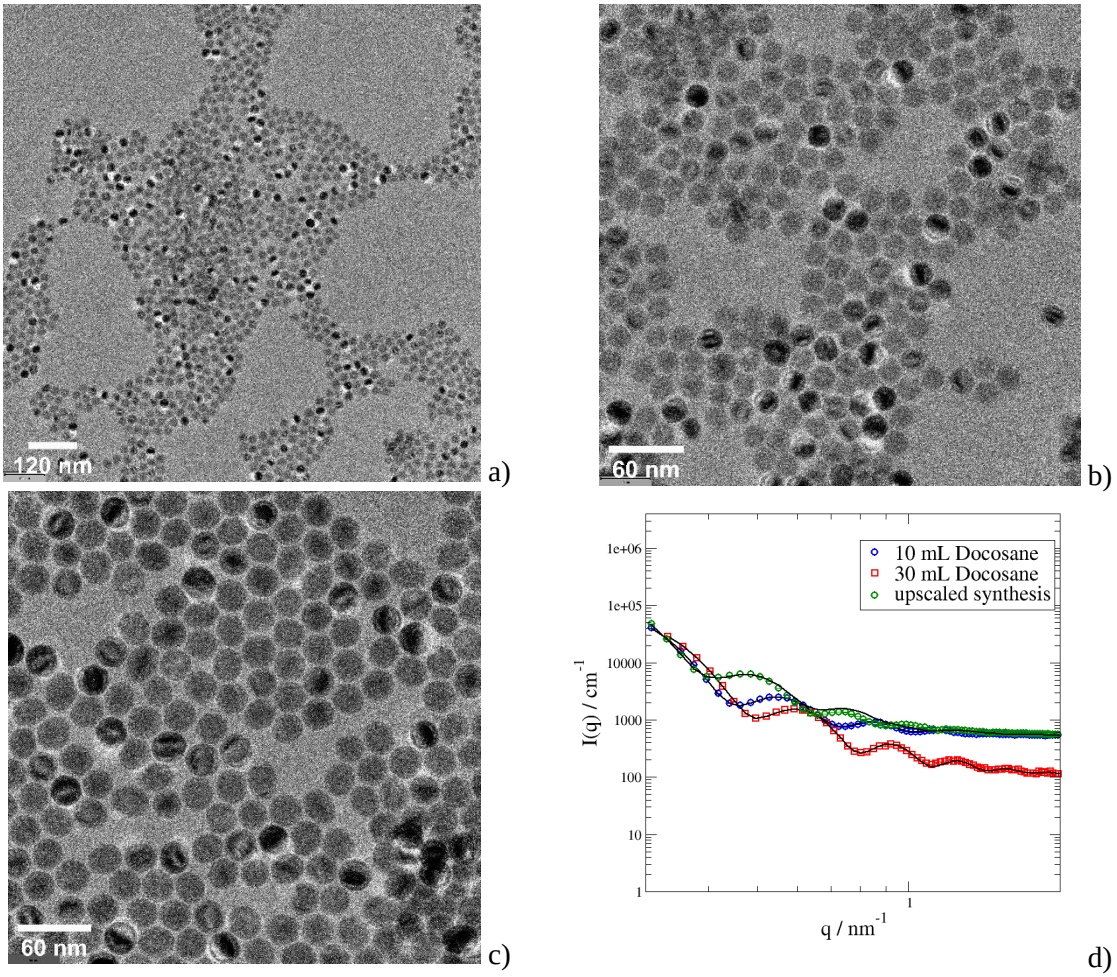

Figure 10. TEM images of iron oxide nanoparticles formed in a) 30 mL docosane, b) 10 mL docosane, c) and upscaled to 4 times the amount of synthesis solution. d)) shows the measured SAXS curves of the synthesized nanoparticles together with core/shell model fits indicated by the solid lines. The determined core radii are R_c = 10.5 nm (blue curve), 9.8 nm (red curve) and 12.1 nm (green curve) respectively.

Trioctylamine

It is possible to obtain > 20 nm diameter SPIONs with a major fraction of magnetite by using trioctylamine as a high boiling point solvent (TOA, bp = 366 °C). It was mentioned as one of the possibilities to synthesize larger nanoparticles[4,17,18] , but we found that all suggested procedures mostly lead to formation of either cubic or extremely polydisperse SPIONs. We checked several reaction temperatures to find out the optimal one to obtain spherical iron oxide nanoparticles. The synthesis was performed at the standard precursor concentration (20 mmol) and heating rate (3.3°C/min). At the standard reaction end temperature (320 °C) only SPIONs with broad size distribution (6.3 nm average radius) can be obtained (Fig. 11 a). Changing the end temperature to 340 °C makes particles more

monodisperse, yielding nanoparticles of 7.0 nm radius (Fig. 11 b). Further raising the temperature up to 370 °C, allows to obtain SPIONs with 10.0 nm radius (Fig. 11 c).

It shows that the final plateau temperature of the reaction is a crucial parameter for size tuning and can be varied to obtain nanoparticles with good size control. A similar result was achieved by Ahmadpoor and collegues[19] who performed the synthesis at 360 °C and obtained 18 nm diameter spherical iron oxide particles, which fits our results very well. The increased size at a temperature of 370°C likely is due to an increased growth rate. The synthesis procedure with trioctylamine as a solvent can provide a variety of monodisperse spherical particles in a size range 11-20 nm and provides an easier purification step in comparison to nanoparticles synthesized in docosane. Also, the nanoparticles synthesized in trioctylamine have a magnetite phase and a monocrystalline structure (Fig. 9c).
A notable effect for nanoparticle synthesis at temperatures at or above the boiling point of the solvent is that nanoparticles with lower size distribution are obtained. This effect is described in detail by Lynch and colleagues [20], who report that either gas bubbles appearing during solvent boiling or the Ar-gas flow can be used to tailor the kinetics of the nucleation and growth.

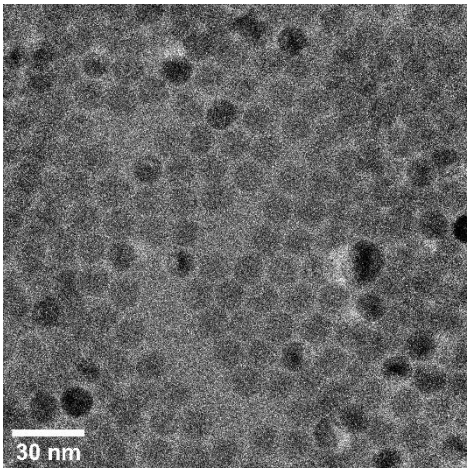

a)

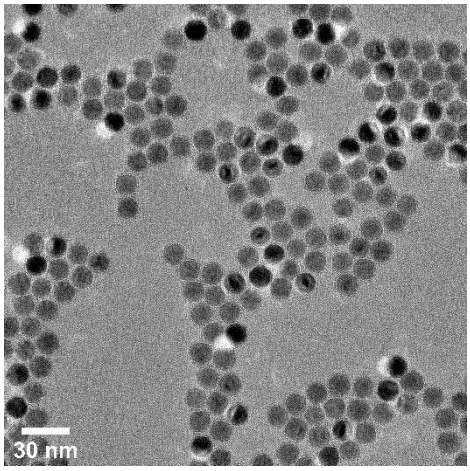

b)

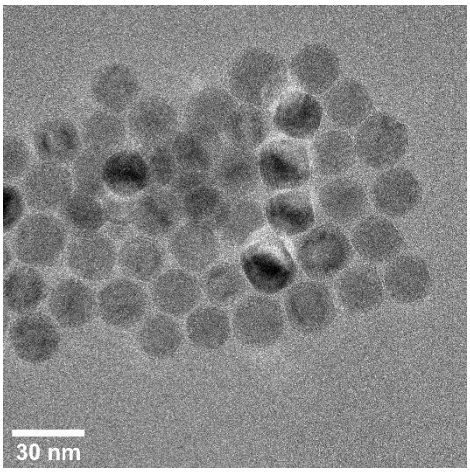

c)

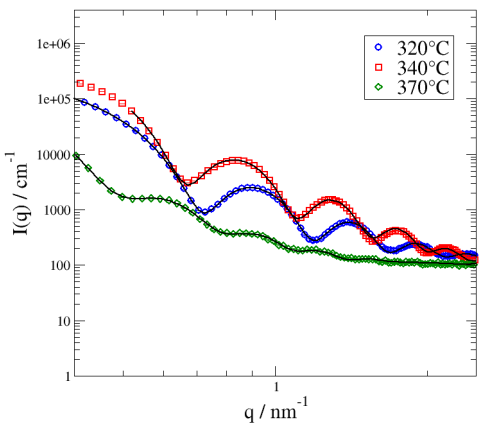

d)

Figure 11. TEM images of iron oxide nanoparticles formed in trioctylamine at the end temperatures of a) 320 °C, b) 340 °C, c) 360 °C. d) shows the measured SAXS curves of the synthesized nanoparticles together with core/shell model fits indicated by the solid lines. The determined core radii are R_c = 6.4 nm (blue curve), 7.0 nm (red curve) and 10.0 nm (green curve), respectively.

4. CONCLUSIONS

We provided an overview over suitable methods and conditions to control the size of iron oxide (SPION) nanoparticles via the variation of the main synthesis parameters. We find that a set of solvents, 1-octadecene, trioctylamine, and docosane, provides access over temperature ranges from start-temperatures of 100°C to end-temperatures of up to 370°C, allowing to synthesize monodisperse nanoparticles in a diameter range of 6 – 24 nm on large scale. We observe that each solvent provides access to a certain temperature range, within which the variation of temperature, heating rate, type of ligand (oleic acid, TOP) or precursor concentration allows to reproducibly vary and fine-control the nanoparticle size to $\pm$0.5 nm as shown in Fig. 12. For each solvent the highest temperature is given by the respective boiling temperature, which are 315°C for 1-octadence, 365°C for trioctylamine, and 369°C for n-docosane.

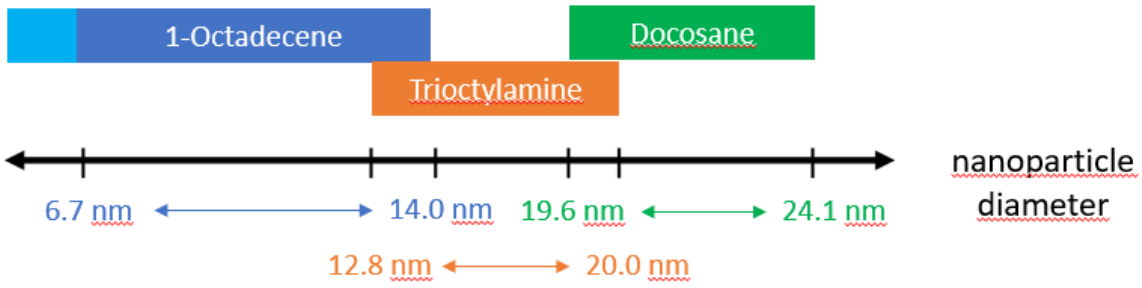

Figure 12. Chart of suitable solvents to access a broad range of iron oxide nanoparticle diameters with narrow size distribution, high crystallinity and a reproducible size control of $\pm$0.5 nm. The light blue area for 1-octadecene shows the range accessible with pristine iron oleate precursor, where the reproducibility is reduced.

With knowledge of the nucleation and growth kinetics it is possible to better rationalize the effects of the variation of the synthesis parameters. We therefore measured the nucleation and growth kinetics by time-resolved SAXS-experiments as shown in Figs. 1 and 2 to make a connection to the detailed description in ref. [6] An increase of the reaction temperature or precursor concentration increases the growth rate, such that larger nanoparticles are obtained. Lower heating rates lead to larger nanoparticles, because nucleation starts at lower temperatures, where the nucleation rate and thus the number of

formed nuclei is smaller. The ligand binding strength has an influence at many steps of the nucleation and growth process, i.e. on the stability and dissolution kinetics of the amorphous precursor phase, and on the nucleation rate, the monomer growth and aggregation rate of the crystalline nanoparticles. It seems that the lower binding strength of oleic acid promotes a high precursor dissolution rate and therefore a high nucleation rate resulting in smaller nanoparticles. Trioctylphosphine and oleylamine seem to bind stronger and thus the dissolution and nucleation rates are slower. We confirm that a thermal pretreatment of the iron oxide precursor is essential to achieve reproducible size control. The annealing time should be just long enough to complete nanoparticle growth. Our investigations thus provide an understanding and a guideline to choose the best synthesis procedure for reproducible size control of monodisperse iron oxide nanoparticles in a size range of 6 – 24 nm.

ASSOCIATED CONTENT

Supporting Information

The Supporting Information is available free of charge at https:/…

Nucleation and growth model; influence of potassium oleate on iron oleate quality and resultant particle size

AUTHOR INFORMATION

Corresponding Authors

Sascha Ehlert – Forschungszentrum Jülich, 52428 Jülich, Germany, orcid: 0000-0002-3408-181X, Email: s.ehlert@fz-juelich.de

Stephan Förster – Forschungszentrum Jülich, 52428 Jülich, Germany, orcid: 0000-0002-7323-2449, Email: s.foerster@fz-juelich.de

Notes

The authors declare no competing financial interest.

REFERENCES

(1) Ali, A.; Shah, T.; Ullah, R.; Zhou, P.; Guo, M.; Ovais, M.; Tan, Z.; Rui, Y. K. Review on Recent Progress in Magnetic Nanoparticles: Synthesis, Characterization, and Diverse Applications. *Front Chem* **2021**, *9*, 548. https://doi.org/10.3389/FCHEM.2021.629054/BIBTEX.

(2) Park, J.; An, K.; Hwang, Y.; Park, J. E. G.; Noh, H. J.; Kim, J. Y.; Park, J. H.; Hwang, N. M.; Hyeon, T. Ultra-Large-Scale Syntheses of Monodisperse Nanocrystals. *Nat Mater* **2004**, *3* (12), 891–895. https://doi.org/10.1038/NMAT1251.

(3) Biehl, R. Jscatter, a Program for Evaluation and Analysis of Experimental Data. *PLoS One* **2019**, *14* (6). https://doi.org/10.1371/JOURNAL.PONE.0218789.

(4) Park, J.; An, K.; Hwang, Y.; Park, J. E. G.; Noh, H. J.; Kim, J. Y.; Park, J. H.; Hwang, N. M.; Hyeon, T. Ultra-Large-Scale Syntheses of Monodisperse Nanocrystals. *Nature Materials 2004 3:12* **2004**, *3* (12), 891–895. https://doi.org/10.1038/nmat1251.

(5) Guinier, A. *Small-Angle Scattering of X-Rays*; Wiley: New York, 1955.

(6) Leffler, V.; Ehlert, S.; Förster, B.; Dulle, M.; Förster, S. Nanoparticle Heat-Up Synthesis: In Situ X-Ray Diffraction and Extension from Classical to Nonclassical Nucleation and Growth Theory. *ACS Nano* **2021**, *15* (1), 840–856. https://doi.org/10.1021/ACSNANO.0C07359/ASSET/IMAGES/LARGE/NN0C07359_0009.JPEG.

(7) Roca, A. G.; Morales, M. P.; Serna, C. J. Synthesis of Monodispersed Magnetite Particles From Different Organometallic Precursors. *IEEE Trans Magn* **2006**, *42* (10), 3025–3029. https://doi.org/10.1109/TMAG.2006.880111.

(8) Yu, W. W.; Falkner, J. C.; Yavuz, C. T.; Colvin, V. L. Synthesis of Monodisperse Iron Oxide Nanocrystals by Thermal Decomposition of Iron Carboxylate Salts{. https://doi.org/10.1039/b409601k.

(9) Hufschmid, R.; Arami, H.; Ferguson, R. M.; Gonzales, M.; Teeman, E.; Brush, L. N.; Browning, N. D.; Krishnan, K. M. Synthesis of Phase-Pure and Monodisperse Iron Oxide Nanoparticles by Thermal Decomposition. *Nanoscale* **2015**, *7* (25), 11142–11154. https://doi.org/10.1039/C5NR01651G.

(10) Balakrishnan, T.; Lee, M.-J.; Choi, S.-M. Cite This: CrystEngComm. **2019**, *21*, 4063. https://doi.org/10.1039/C9CE00112C.

(11) Bronstein, L. M.; Huang, X.; Retrum, J.; Schmucker, A.; Pink, M.; Stein, B. D.; Dragnea, B. Influence of Iron Oleate Complex Structure on Iron Oxide Nanoparticle Formation. *Chemistry of Materials* **2007**, *19* (15), 3624–3632. https://doi.org/10.1021/CM062948J/SUPPL_FILE/CM062948JSI20070423_032524.PDF.

(12) Cotin, G.; Perton, F.; Petit, C.; Sall, S.; Kiefer, C.; Begin, V.; Pichon, B.; Lefevre, C.; Mertz, D.; Greneche, J. M.; Begin-Colin, S. Harnessing Composition of Iron Oxide Nanoparticle: Impact of Solvent-Mediated Ligand-Ligand Interaction and Competition between Oxidation and Growth Kinetics. *Chemistry of Materials* **2020**, *32* (21), 9245–9259. https://doi.org/10.1021/ACS.CHEMMATER.0C03041/SUPPL_FILE/CM0C03041_SI_001.PDF.

(13) Alexey Shavel and Luis M. Liz-Marzán. Shape Control of Iron Oxide Nanoparticles. *Physical Chemistry Chemical Physics* **2009**, *11* (19), 3762–3766. https://doi.org/10.1039/B822733K.

(14) Demortière, A.; Panissod, P.; Pichon, B. P.; Pourroy, G.; Guillon, D.; Donnio, B.; Bégin-Colin, S. Size-Dependent Properties of Magnetic Iron Oxide Nanocrystals. *Nanoscale* **2011**, *3* (1), 225–232. https://doi.org/10.1039/C0NR00521E.

(15) Lak, A.; Kraken, M.; Ludwig, F.; Kornowski, A.; Eberbeck, D.; Sievers, S.; Litterst, F. J.; Weller, H.; Schilling, M. Size Dependent Structural and Magnetic Properties of FeO–Fe3O4 Nanoparticles. *Nanoscale* **2013**, *5* (24), 12286–12295. https://doi.org/10.1039/C3NR04562E.

(16) Tancredi, P.; Rojas, P. C. R.; Moscoso-Londoño, O.; Wolff, U.; Neu, V.; Damm, C.; Rellinghaus, B.; Knobel, M.; Socolovsky, L. M. Synthesis Process, Size and Composition Effects of Spherical Fe 3 O 4 and FeO@Fe 3 O 4 Core/Shell Nanoparticles. *New Journal of Chemistry* **2017**, *41* (24), 15033–15041. https://doi.org/10.1039/C7NJ02558K.

(17) Glasgow, W.; Fellows, B.; Qi, B.; Darroudi, T.; Kitchens, C.; Ye, L.; Crawford, T. M.; Mefford, O. T. Continuous Synthesis of Iron Oxide (Fe3O4) Nanoparticles via Thermal Decomposition. *Particuology* **2016**, *26*, 47–53. https://doi.org/10.1016/J.PARTIC.2015.09.011.

(18) Kumar, D.; Singh, H.; Jouen, S.; Hannoyer, B.; Banerjee, S. Effect of Precursor on the Formation of Different Phases of Iron Oxide Nanoparticles. *RSC Adv* **2015**, *5* (10), 7138–7150. https://doi.org/10.1039/c4ra10241j.

(19) Ahmadpoor, F.; Masood, A.; Feliu, N.; Parak, W. J.; Shojaosadati, S. A. The Effect of Surface Coating of Iron Oxide Nanoparticles on Magnetic Resonance Imaging Relaxivity. *Frontiers in Nanotechnology* **2021**, *3*, 13. https://doi.org/10.3389/FNANO.2021.644734/BIBTEX.

(20) Lynch, J.; Zhuang, J.; Wang, T.; Lamontagne, D.; Wu, H.; Cao, Y. C. Gas-Bubble Effects on the Formation of Colloidal Iron Oxide Nanocrystals. *J Am Chem Soc* **2011**, *133* (32), 12664–12674. https://doi.org/10.1021/JA2032597/SUPPL_FILE/JA2032597_SI_001.PDF.